

PLASTIC COVER GREENHOUSES REFLECTANCE SPECTRA FROM DIFFERENT OPTICAL SATELLITE IMAGERY

R. Jiménez-Lao¹, M.A. Aguilar^{1,*}, F.J. Aguilar¹

¹ University of Almería. Department of Engineering and Research Centre CIAIMBITAL. Almería 04120, Spain.
(rjl020, maguilar, faguilar)@ual.es

Commission II, WG II/6

KEY WORDS: Plastic Covered Greenhouses, Reflectance, Spectral Indexes, OBIA, Landsat 8, WorldView-3, Sentinel-2.

ABSTRACT:

Mapping the distribution of plastic covered greenhouses (PCG) is essential for any attempts to manage these complex areas of intensive agriculture. It is therefore important to understand how the spectrum of different PCG varies in order to establish its unique absorption features and how these can be utilised for mapping PCG from remote sensing imagery. This paper presents an analysis of the surface reflectance values of satellite image spectra for 50 PCG. The reflectance of these PCG, located in Almería (Spain), was studied in two seasons of the year (summer and winter). All single bands of WorldView-3 (WV3), Sentinel-2 MSI (S2 L2A) and Landsat 8 OLI (L8 L2), together with Normalized Difference Plastic Index (NDPI) and Normalized Difference Vegetation Index (NDVI), were generated through an object-based image analysis (OBIA) approach for each PCG and season. The results showed the variability of absorption features and overall shape of the spectra for all PCG. The main differences in reflectance were attributed to the crops and the specific characteristics of their local management. A relationship between brightness and whitewashing (greenhouse roof painted with lime to provide shade and reduce the temperature inside the greenhouse, especially in summer) was found, showing the ability of whitewashing to temporally mask the spectral signature of the plastic film.

1. INTRODUCTION

Greenhouse farming is an agricultural management system that has demonstrated its efficiency in intensifying food production. These systems constitute a feasible alternative to ensure food supply, one of the greatest challenges facing humanity in the 21st century (Aznar-Sánchez et al., 2020).

The province of Almería, located in the semi-arid coastal plain of Southeast Spain, has a plastic covered greenhouses (PCG) area of 31,614 ha and an even larger crop-growing surface (45,680 ha), thanks to the scheduling of two growing cycles per year. Over the last 18 years, PCG surface area has increased by 16%. These data make Almería the province with the highest concentration of protected crop surface (greenhouses) in the world (Duque-Acevedo et al., 2020). This large concentration of PCG requires transformative solutions for social, economic and environmental challenges and processes (Castro et al., 2019). Remote sensing provides coverage of large areas with high precision and can be a very efficient tool for improved management across scales (Segarra et al., 2020).

Periodic spectral data in the visible and infrared part of the electromagnetic spectrum (VNIR), acquired from various satellite sensors, offers an unlimited basic source of information (Pleniou and Koutsias, 2013). Remote sensing is the most cost-effective method for large scale monitoring and analyses in agriculture. To date, the main remote sensing tools utilized by the agricultural sector are visible, near infrared (NIR), and short-wave infrared (SWIR) sensors (Khanal et al., 2017).

Several research lines have emerged throughout the 21st century based on emerging satellite data sources. As an alternative to pixel-based modelling, object-based image analysis (OBIA) provides a framework that can be used to integrate more complex

data than the raw remote sensing signal by including different levels of spatial information (de Grandpré et al., 2022; Hossain and Chen, 2019; Jiménez-Lao et al., 2020). Spectral indexes represent one of the most used approaches to analyse data in the optical domain. However, optimal indexes should be designed for specific applications and particular instruments (Verstraete and Pinty, 1996).

This work aims at exploring and characterizing the spectral properties of PCG by comparing the reflectance values of three different optical satellite sensors such as WorldView-3, Sentinel-2 and Landsat 8. The mean reflectance values of each single band, brightness computed from RGB bands, as well as Normalized Difference Vegetation Index (NDVI) and Normalized Difference Plastic Index (NDPI), were studied for 50 units of PCG and two seasons (winter and summer).

2. STUDY SITE AND DATASETS

2.1 Study Site

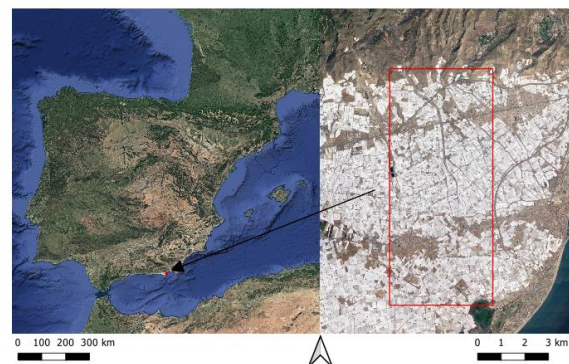


Figure 1. Location of the study area.

* Corresponding author

This investigation was conducted in Almería, located in the Southeast of Spain, specifically over an area with a great concentration of PCG. The study site comprised a rectangle area of about 5,000 ha centred on the WGS84 geographic coordinates of 36.7824°N and 2.6867°W (Fig. 1).

2.2 Data set Pre-processing

Seven cloud-free satellite images were acquired in 2020. They were taken in two dates (summer and winter) from three different sensors: WorldView-3 (WV3), Landsat 8 (L8) and Sentinel-2 (S2). S2 data include both Sentinel-2A and 2B images.

Two WV3 bundle images in Ortho Ready Standard Level-2A (ORS2A) format including 16 bands (panchromatic (PAN) with 0.3 m ground sample distance (GSD), multispectral (MS) with 1.2 m GSD, and short-wave infrared (SWIR) with 3.7 m GSD) were acquired on July 11 and December 25, respectively (Table 1). A pansharpened image with 0.3 m GSD was attained by means of the PANSHARP module included in Geomatica v. 2018 (PCI Geomatics, Richmond Hill, ON, Canada) from the PAN and MS images of WV3. For the two images, the coordinates of seven ground control points (GCPs), obtained by differential global positioning systems (DGPS), were used to compute the sensor model based on rational functions refined by a zero-order transformation in the image space (RPC0). A medium resolution 10 m grid spacing DEM with a vertical accuracy of 1.34 m (root mean square error (RMSE)), provided by the Andalusian Government, was used to carry out the orthorectification process. Two WV3 orthoimages with 3.7 m GSD containing all the 16 bands were generated using Geomatica v. 2018. Finally, the orthoimages were atmospherically corrected by using the ATCOR (atmospheric correction) module included in Geomatica v. 2018. This absolute atmospheric correction algorithm involves the conversion of the original raw digital numbers to ground reflectance values by applying the MODTRAN (MODerate resolution atmospheric TRANsmission) radiative transfer code.

Three S2 images in level 2A mode (L2A) were acquired on July 12, December 24 and December 26 from Sentinel-2A, 2B, and 2A, respectively. The L2A product provides surface reflectance images divided in 100 x 100 km² UTM/WGS84 projected tiles. This product has been systematically generated using Sen2Cor processor (Main-Knorn et al., 2015) over Europe since March 2018, and was extended to a global scale in December 2018. The S2 sensor collects up to thirteen bands with three different geometric resolutions ranging from 60 m to 10 m GSD. S2 images were freely downloaded from the European Space Agency (ESA)-Copernicus Scientific Data Hub tool. In this study, six 20 m GSD bands and four 10 m GSD bands were used (Table 1). These images were clipped according to the study area. Next they were co-registered with the WV3 pansharpened orthoimages (0.3 m GSD) using a first order polynomial transformation computed on 10 planimetric GCPs evenly distributed over the study area.

Two L8 (Collection 1 Level-2 (L2) products) images were acquired on July 11 and December 29. They were freely downloaded from the U.S. Geological Survey (USGS) website through the EarthExplorer tool. The L8 OLI L2 product is considered as the official surface reflectance product for L8 images. It is generated through the LaSRC code (Vermote et al., 2016) at 30 m GSD (Table 1). These images were clipped according to the corresponding study area. After that, they were co-registered in the same way that the S2 images.

A detailed view of six out of the seven images used in this work can be seen in Figure 2. In the case of S2, we decided to use two images for the summer season. Each pair of scenes was taken on the same day (preferably) or with and acquisition time difference ranging from 1 to four days.

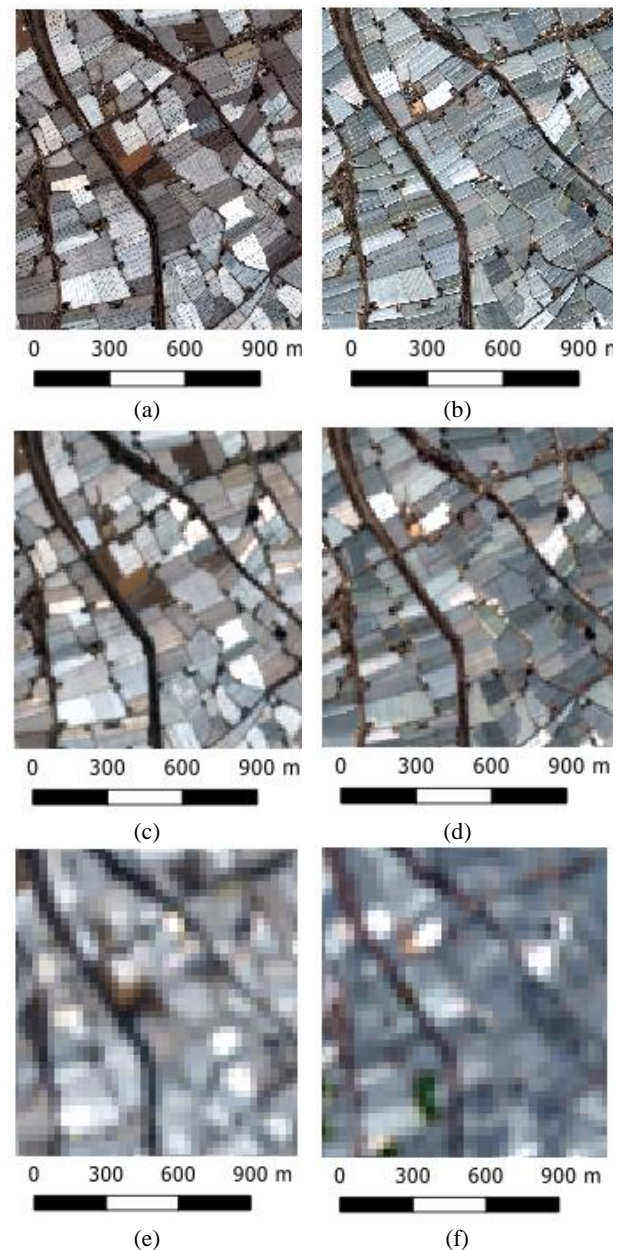


Figure 2. Detailed view (RGB) of six of the images used in this work: (a) WV3 3.7 m GSD, July 11; (b) WV3 3.7 m GSD, December 25; (c) S2 10 m GSD, July 12; (d) S2 10 m GSD, December 24; (e) L8 30 m GSD, July 11; (f) L8 30 m GSD, December 29.

WorldView-3		
Name	Range (nm)	Resolution (m)
Coastal	397–454	1.2
Blue	445–517	1.2
Green	507–586	1.2
Yellow	580–629	1.2
Red	626–696	1.2
Red Edge	698–749	1.2
NIR1	765–899	1.2
NIR2	857–1039	1.2
SWIR9	1184–1235	3.7
SWIR10	1546–1598	3.7
SWIR11	1636–1686	3.7
SWIR12	1702–1759	3.7
SWIR13	2137–2191	3.7
SWIR14	2174–2232	3.7
SWIR14	2228–2292	3.7
SWIR16	2285–2373	3.7
Sentinel-2		
Name	Range (nm)	Resolution (m)
Blue	458-523	10
Green	543-578	10
Red	650-680	10
Red Edge 1 (RE1)	698-713	20
Red Edge 2 (RE2)	733-748	20
Red Edge 3 (RE3)	773-793	20
NIR8	785-899	10
NIR8a	855-875	20
SWIR1	1565-1655	20
SWIR2	2100-2280	20
Landsat 8 OLI		
Name	Range (nm)	Resolution (m)
Coastal	435-451	30
Blue	452-512	30
Green	533-590	30
Red	636-673	30
NIR	851-879	30
SWIR1	1566-1651	30
SWIR2	2107-2294	30

Table 1. Bands of WorldView-3, Sentinel-2, and Landsat 8 OLI used in this study.

3. METHODOLOGY

In this study, spectral signatures collected from WV3, S2 and L8 images were first analysed to identify spectral difference in single bands over PCG land cover. In addition, NDVI (Rouse et al., 1973) and NDPI (Guo and Li, 2020) were evaluated. Note that NDPI is a novel spectral index for detecting plastic materials based on WV3 SWIR bands.

The reflectance spectra were evaluated using 50 well-distributed polygons over the study site, all of them located inside of individual PCG. These 50 manually segmented objects were delineated onto the WV3 pansharpened image. Furthermore, each polygon was digitized, adapting its boundary to the shape of each PCG and leaving an inside buffer of at least 10 m. This technique tried to avoid potentially mixed pixels located at the edges of the sampled PCG, which is a very usual issue when working on medium-resolution satellite imagery (Aguilar et al., 2020).

Trimble eCognition Developer v. 9.4 software was employed for the extraction of the mean surface reflectance values of all the pixels inside of each reference surface polygon from WV3, S2 and L8

products. To do this, the chessboard segmentation algorithm included in eCognition was applied to a previously digitized thematic layer containing the 50 reference polygons. Through using this approach, the software only projects the vector file onto the images in order to obtain a boundary adapted to the pixels (sample) to be extracted inside the polygons. One eCognition project was conducted for each image and date (i.e., seven different projects were carried out). Figure 3 depicts the 50 reference PCG polygons in blue, which were manually digitized on the WV3 pansharpened image generated on July 11.

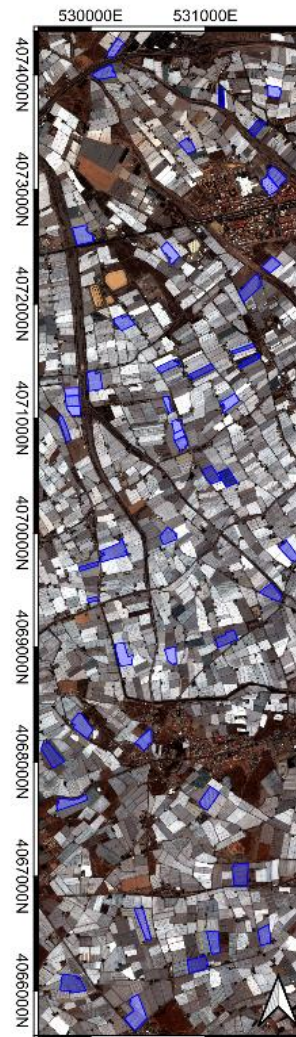


Figure 3. Reference PCG in blue over WV3 July 11.

Finally, the mean surface reflectance values (digital numbers ranging from 0 to 10,000) were extracted for each one of the WV3, S2 and L8 bands shown in Table 1 for the two seasons tested. All the pixels (with an enhanced spatial resolution of about 1 m) within the OBIA segments were considered. NDVI and NDPI were also computed for each polygon and date, using the mean values attained from Red and NIR bands (NIR8a for S2 and NIR2 for WV3) and SWIR bands of WV3 (SWIR10, SWIR12, SWIR13 and SWIR16) (Equations 1 and 2).

It is important to note that NDPI only was computed for WV3 images, while NDVI was calculated in all cases. Figure 4 shows

the flowchart that summarizes the method applied to obtain the features extracted from each reference polygon.

$$NDVI = \frac{(NIR - R)}{(NIR + R)} \quad (1)$$

$$NDPI = \frac{(SWIR10 - SWIR12) + (SWIR13 - SWIR16)}{(SWIR10 + SWIR12) + (SWIR13 + SWIR16)} \quad (2)$$

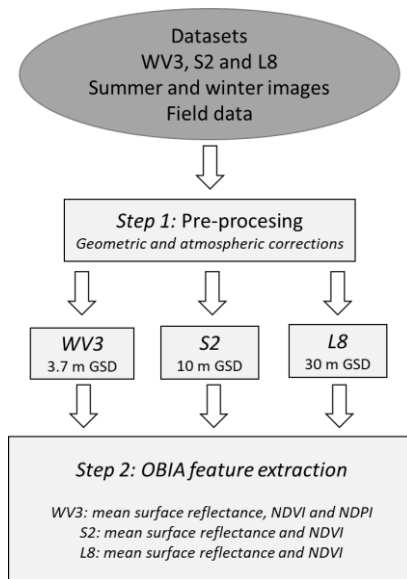


Figure 4. Flowchart of the methodology applied in this work.

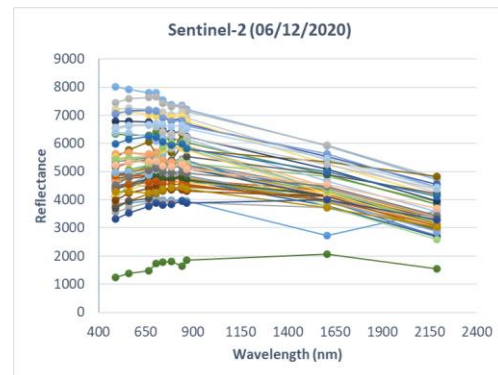
4. RESULTS AND DISCUSSION

4.1 Spectral properties of PCG

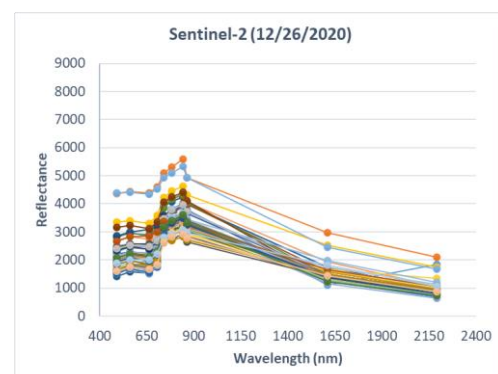
The reflectance values for each spectral band (following the order depicted in Table 1 for each satellite) extracted from the sample of 50 PCG, including summer and winter data, are presented in Figure 5, Figure 6 and Figure 7 for S2, WV3 and L8 sensors, respectively. As it was described above, the spectral signatures of PCG were compared in two periods to obtain a better understanding of their spectral behaviour and potential discriminatory ability. According to Guo and Li (2020), the discrimination provided by the NIR and SWIR spectral channels is usually greater than that obtained by using only the visible bands.

The spectral behaviour of the two periods turned out to be very similar for the three satellite imagery studied. The spectral signature presented higher variability over the summer period. In this case, the reflectance values ranged from 1,238 to 8,002 digital number (DN) for S2, from 1,340 to 7,081 DN for WV3, and from 2,134 to 4,966 DN for L8 in the blue channel. However, the reflectance values showed narrower variability in the winter season. This fluctuation of the three sensors between periods, due to occasional sun glint effects and the presence of eventual roof greenhouse whitewash (greenhouse shading) that temporally masked the spectral signature of the plastic film, has been already described in Aguilar et al. (2021). In fact, whitewashed agriculture management technique is commonly used to control temperature by decreasing the radiation inside the greenhouse in southern Spain. Note that the energy reflected from the whitewash is not accumulated inside the greenhouse (Fernandez

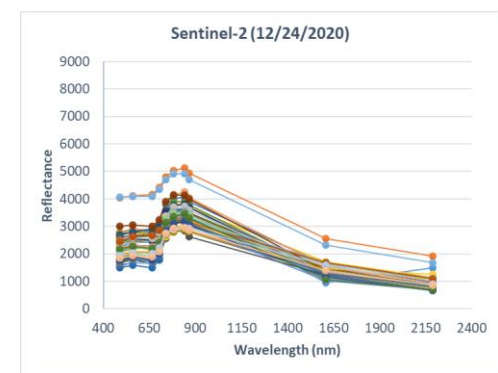
Rodriguez et al., 2003). The advantage of using whitewashed lies mainly in its price and its easy and economical application. Whitewashed is used during the periods of higher radiation, which coincide with summer season in northern hemisphere. This is the reason why more PCG appear with a characteristic white colour in the summer images than in winter ones (Figure 2).



(a)



(b)



(c)

Figure 5. Spectral signature plots extracted from S2 images for each of the 50 PCG samples. (a) Summer period. (b) and (c) Winter period.

It should be noted that the S2, WV3 and L8 images showed higher reflectance values and greater inter-greenhouse variability in summer season than in winter. In the same way, the shape of the spectral signature for visible and near-infrared channels turned out to be more similar to the typical shape of outdoor crops during the winter period, just when the crop is usually fully developed (higher leaf area index) and greenhouse roofs are cleaner to increase the luminosity (especially photosynthetically active radiation (PAR)) inside the greenhouse.

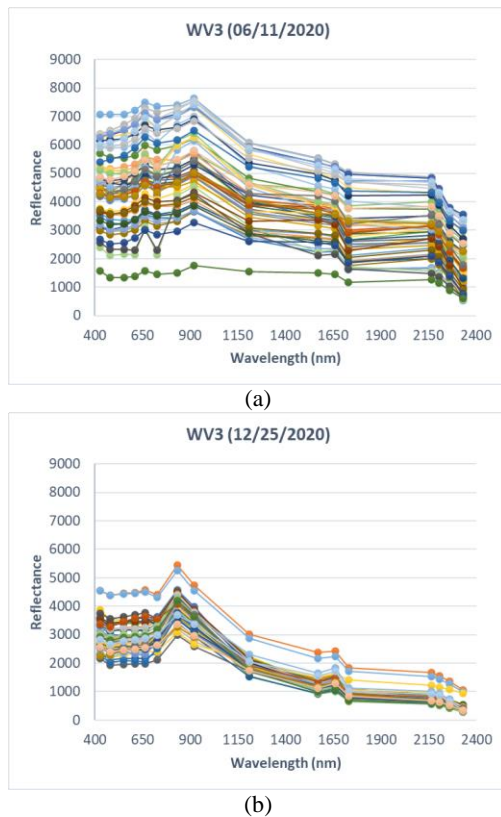


Figure 6. Spectral signature plots extracted from WV3 images for each of the 50 PCG samples. (a) Summer period. (b) Winter period.

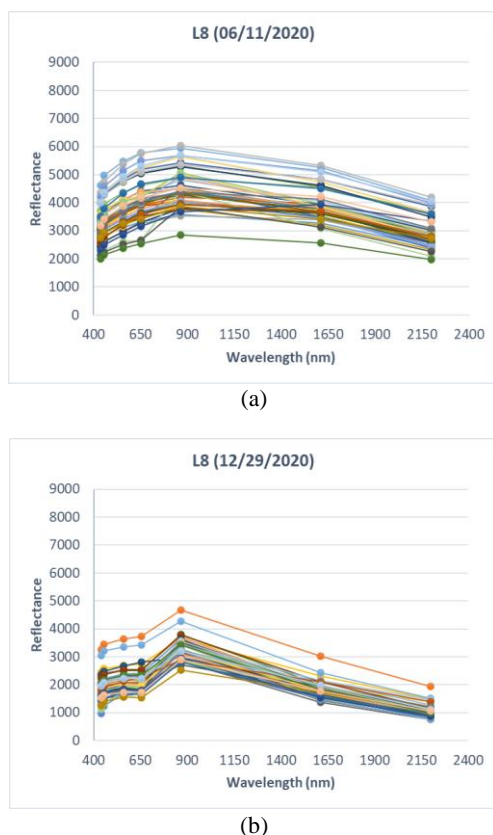


Figure 7. Spectral signature plots extracted from L8 images for each of the 50 PCG samples. (a) Summer period. (b) Winter period.

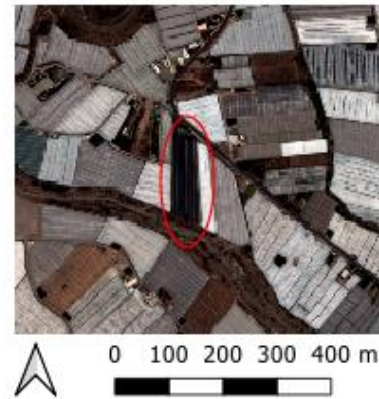


Figure 8. Greenhouse with black shading net marked with a red ellipse over a WV3 image taken on July 11.

Observing the spectral signatures of the three sensors in the summer period (Fig. 5a, 6a and 7a), it can be made out a spectral signature with clearly lower values (represented in green). It corresponds to a greenhouse with a black shading net. This greenhouse is shown in Figure 8. During winter period (Fig. 5b, 5c, 6b and 7b), we found two objects that, especially through the visible spectrum, had higher reflectance values than the rest. They are represented in orange and blue colours. This occurred for all three sensors tested. It is important to highlight that these are greenhouses that were whitewashed during the winter period to limit the vegetative growth of the crop (Figure 9).

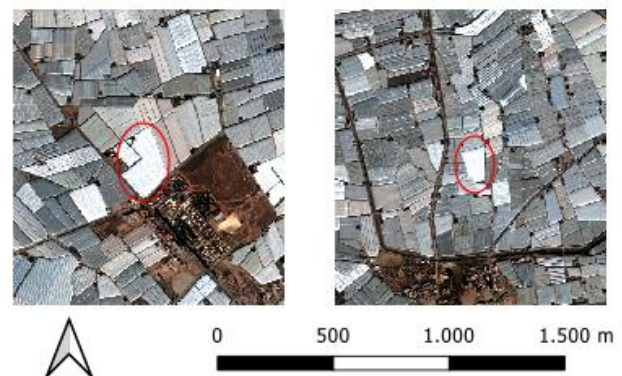


Figure 9. Whitewashed greenhouses marked with red ellipses over a WV3 image taken on December 25.

4.2 Visual evaluation

NDVI has been a principal vegetation index in multi-temporal vegetation monitoring, providing a quantitative value of the spectral contrast between red and near infrared surface reflectance (Tucker, 1979). The NDVI values obtained during winter were higher than those obtained during summer. False-colour satellite images from WV3 (NIR1-Red-Green), S2 (NIR8a-Red-Green) and L8 (NIR-Red-Green) (Figure 10) show a clearly light pink greenhouse colour over all satellite images in winter period. That is just when greenhouse cultivation was growing and, in most cases, fully developed.

4.3 Analysis Based on Indices

To analyse the whitewashing on the greenhouses through satellite images, the brightness feature has been used. It was computed as the average of the visible (RGB) bands.

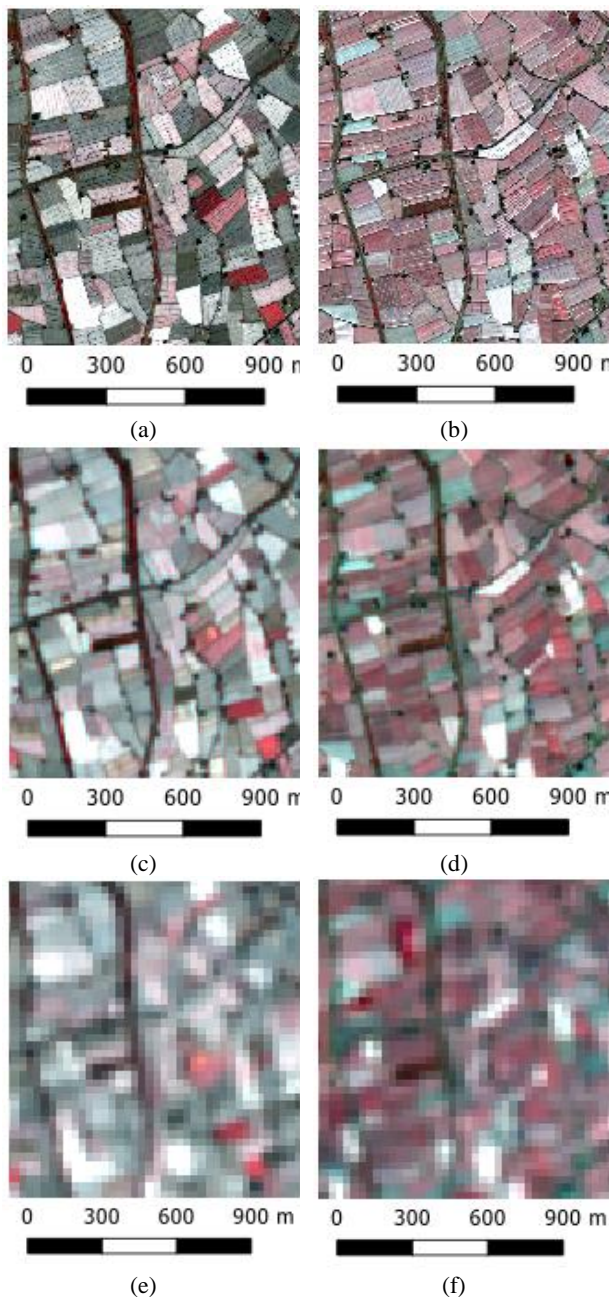


Figure 10. False-colour satellite images: (a) WV3 July 11; (b) WV3 December 26; (c) S2 July 12; (d) S2 December 24; (e) L8 July 11; (f) L8 December 29.

In Figure 11, we can see the scatterplots relating NDPI and brightness values calculated on WV3 images for each PCG in summer period (Fig. 10a) and winter period (Fig. 10b). The relationship between brightness and NDPI values shows that high brightness values are related to low NDPI values in summer (Figure 11a). Overall, the whitewashed masked the plastic properties of PCG provoking that NDPI (plastic index) was much lower. It is noteworthy that, in Figure 11a, the point that had a lower brightness, which is more displaced to the left, was the greenhouse represented in Figure 8. Its unique characteristic black colour produced lower values in the visible spectrum (low brightness), although it could be successfully detected by applying the NDPI index (i.e., this greenhouse had a plastic roof).

During the winter period, when the practice of whitewashed is not usually applied, the NDPI values looked like more stable. Two greenhouses, those represented in Figure 9, presented clearly higher brightness due to whitewashed.

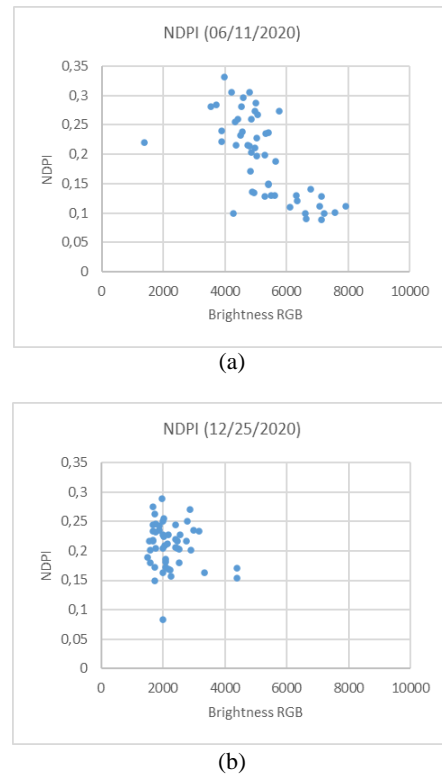


Figure 11. Scatterplots relating NDPI and brightness values for WV3 and each PCG in (a) Summer and (b) Winter.

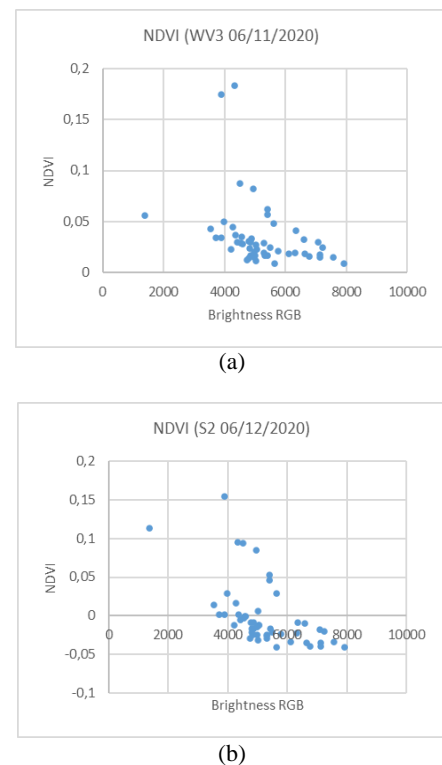


Figure 12. Scatterplots relating NDVI and brightness values computed on a) WV3 and (b) S2 images for each PCG in summer.

The scatterplots relating NDVI and brightness values computed on WV3 and S2 for each PCG in summer are depicted in Figure 12. During the summer months, greenhouses, in addition to being mostly whitewashed, do not house growing crops or they are in very early stages. So, the NDVI values are usually very low. Note that in summer period it is even possible to find negative NDVI values, mainly when calculating this index from S2 data. Those negative values are attributed to the glint effect described in Aguilar et al. (2020).

The corresponding NDVI and brightness values for the winter season are presented in Figure 13. The NDVI values followed a clear tendency to decrease when the brightness values increased for both WV3 (Figure 13a) and S2 (Figure 13b) sensors.

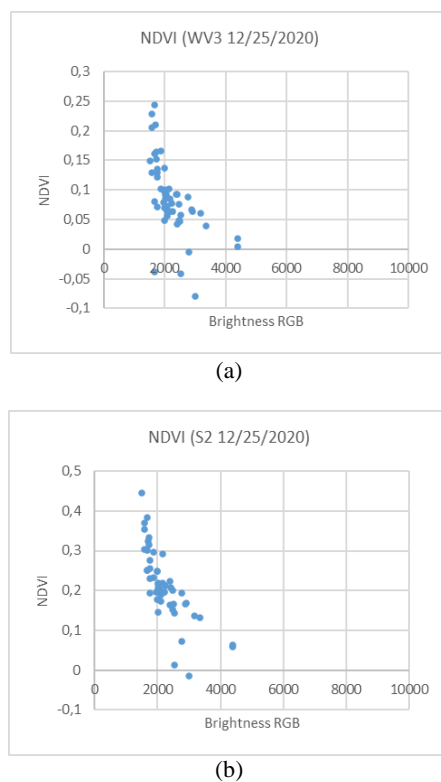


Figure 13. Scatterplots relating NDVI and brightness values calculated on WV3 (a) and S2 (b) imagery for each PCG in winter.

5. CONCLUSIONS

In this study, an OBIA analysis of the reflectance values obtained by three different sensors (WV3, S2 and L8) over PCG landcover was carried out.

When observing the extracted reflectance values, the first finding that stands out is the different spectral capacity of each of the sensors, being WV3 the sensor that collects the most wavelengths with the highest resolution (16 bands with a maximum 3.7 m GSD). On the other hand, the results obtained in the 50 PCG objects analysed show a concordance between the three sensors, which could lead to future studies in which they could be used together.

It was observed a high variability between the objects classified as greenhouses in the study area. In this sense, there is a need to perform a previous clustering-based classification to

differentiate, at least, whitewashed and black shading net greenhouses due to their extremely singular spectral response. Further studies undertaken in different study areas will allow a better understanding of the common spectral aspects of greenhouses over the world.

Finally, the agricultural practice of greenhouse bleaching or whitewashing masked the original spectral properties of the greenhouse cover plastic. For a better understanding of this effect, further studies on both spatial and temporal brightness variability on greenhouses and its relationship with whitewashing should be carried out.

ACKNOWLEDGEMENTS

We acknowledge the support of the Spanish Ministry for Science, Innovation and Universities (Spain) and the European Union (European Regional Development Fund, ERDF) funds (Grant Reference RTI2018-095403-B-I00). It takes part of the general research lines promoted by the Agrifood Campus of International Excellence ceiA3 (<http://www.ceia3.es/>).

REFERENCES

Aguilar, M.A., Jiménez-Lao, R., Aguilar, F.J., 2021. Evaluation of object-based greenhouse mapping using worldview-3 vnr and swir data: A case study from almería (spain). *Remote Sensing*, 13(11). <https://doi.org/10.3390/RS13112133>.

Aguilar, M.A., Jiménez-Lao, R., Nemmaoui, A., Aguilar, F.J., Koc-San, D., Tarantino, E., Chourak, M., 2020. Evaluation of the consistency of simultaneously acquired Sentinel-2 and landsat 8 imagery on plastic covered greenhouses. *Remote Sensing*, 12(12). <https://doi.org/10.3390/rs12122015>.

Aznar-Sánchez, J.A., Velasco-Muñoz, J.F., López-Felices, B., Román-Sánchez, I.M., 2020. An Analysis of Global Research Trends on Greenhouse Technology: Towards a Sustainable Agriculture. *International Journal of Environmental Research and Public Health* 2020, Vol. 17, Page 664, 17(2), 664. <https://doi.org/10.3390/IJERPH17020664>.

Castro, A.J., López-Rodríguez, M.D., Giagnocavo, C., Gimenez, M., Céspedes, L., La Calle, A., Gallardo, M., Pumares, P., Cabello, J., Rodríguez, E., Uclés, D., Parra, S., Casas, J., Rodríguez, F., Fernandez-Prados, J.S., Alba-Patiño, D., Expósito-Granados, M., Murillo-López, B.E., Vasquez, L.M., Valera, D.L., 2019. Six Collective Challenges for Sustainability of Almería Greenhouse Horticulture. *International Journal of Environmental Research and Public Health* 2019, Vol. 16, Page 4097, 16(21), 4097. <https://doi.org/10.3390/IJERPH16214097>.

de Grandpré, A., Kinnard, C., Bertolo, A., 2022. Open-Source Analysis of Submerged Aquatic Vegetation Cover in Complex Waters Using High-Resolution Satellite Remote Sensing: An Adaptable Framework. *Remote Sensing*, 14(2), 267. <https://doi.org/10.3390/rs14020267>.

Duque-Acevedo, M., Belmonte-Ureña, L.J., Plaza-Úbeda, J.A., Camacho-Ferre, F., 2020. The Management of Agricultural Waste Biomass in the Framework of Circular Economy and Bioeconomy: An Opportunity for Greenhouse Agriculture in Southeast Spain. *Agronomy* 2020, Vol. 10, Page 489, 10(4), 489. <https://doi.org/10.3390/AGRONOMY10040489>.

Fernandez Rodriguez, E.J., Camacho Ferre, F., Lao Arenas, M. T., Gómez, V.P., Kenig, A., Jiménez, S., 2003. Effects of aluminized shading screens vs whitewash in a non heated greenhouse temperature. *Acta Horticulturae*, 614, 427–432. <https://doi.org/10.17660/ACTAHORTIC.2003.614.64>.

Guo, X., Li, P., 2020. Mapping plastic materials in an urban area: Development of the normalized difference plastic index using WorldView-3 superspectral data. *ISPRS Journal of Photogrammetry and Remote Sensing*, 169, 214–226. <https://doi.org/10.1016/j.isprsjprs.2020.09.009>.

Hossain, M.D., Chen, D., 2019. Segmentation for Object-Based Image Analysis (OBIA): A review of algorithms and challenges from remote sensing perspective. In *ISPRS Journal of Photogrammetry and Remote Sensing* (Vol. 150, pp. 115–134). Elsevier B.V. <https://doi.org/10.1016/j.isprsjprs.2019.02.009>.

Jiménez-Lao, R., Aguilar, F.J., Nemmaoui, A., Aguilar, M.A., 2020. Remote sensing of agricultural greenhouses and plastic-mulched farmland: An analysis of worldwide research. *Remote Sensing*. <https://doi.org/10.3390/RS12162649>

Khanal, S., Fulton, J., Shearer, S., 2017. An overview of current and potential applications of thermal remote sensing in precision agriculture. In *Computers and Electronics in Agriculture* (Vol. 139, pp. 22–32). Elsevier B.V. <https://doi.org/10.1016/j.compag.2017.05.001>.

Main-Knorn, M., Pflug, B., Debaecker, V., Louis, J., 2015. Calibration and validation plan for the L2A processor and products of the Sentinel-2 mission. *Int. Arch. Photogramm. Remote Sens. Spat. Inf. Sci.*, XL-7/W3, 1249–1255. <https://doi.org/10.5194/isprsarchives-XL-7-W3-1249-2015>.

Pleniou, M., Koutsias, N., 2013. Sensitivity of spectral reflectance values to different burn and vegetation ratios: A multi-scale approach applied in a fire affected area. *ISPRS Journal of Photogrammetry and Remote Sensing*, 79, 199–210. <https://doi.org/10.1016/j.isprsjprs.2013.02.016>.

Rouse, W., Haas, R.H., Shell, J.A., Deering, D.W., 1973. Monitoring vegetation systems in the great plains with ERTS. *Proc. Third ERTS Symp. NASA SP-351*. <https://ntrs.nasa.gov/archive/nasa/casi.ntrs.nasa.gov/19740022614.pdf>.

Segarra, J., Buchailot, M.L., Araus, J.L., Kefauver, S.C., 2020. Remote sensing for precision agriculture: Sentinel-2 improved features and applications. In *Agronomy* (Vol. 10, Issue 5). MDPI AG. <https://doi.org/10.3390/agronomy10050641>.

Tucker, C.J., 1979. Red and Photographic Infrared linear Combinations for Monitoring Vegetation. In *REMOTE SENSING OF ENVIRONMENT* (Vol. 8).

Vermote, E., Justice, C., Claverie, M., Franch, B., 2016. Preliminary analysis of the performance of the Landsat 8/OLI land surface reflectance product. *Remote Sens. Environ.*, 185, 46–56. <https://doi.org/10.1016/J.RSE.2016.04.008>.

Verstraete, M. M., Pinty, B., 1996. Designing optimal spectral indexes for remote sensing applications. *IEEE Transactions on Geoscience and Remote Sensing*, 34(5), 1254–1265. <https://doi.org/10.1109/36.536541>.